PHYSICAL REVIEW B **79**, 205106 (2009)

Electronic structure and electron-phonon coupling of doped graphene layers in KC_8

A. Grüneis,[1,2] C. Attaccalite,[3] A. Rubio,[3] D. V. Vyalikh,[4] S. L. Molodtsov,[4] J. Fink,[2,5] R. Follath,[5] W. Eberhardt,[5] B. Büchner,[1] and T. Pichler[1]

[1]*Faculty of Physics, University of Vienna, Boltzmanngasse 5, A-1090 Vienna, Austria*

[2]*IFW Dresden, P.O. Box 270116, D-01171 Dresden, Germany*

[3]*Departamento de Fisica de Materiales, Nano-Bio Spectroscopy Group and European Theoretical Spectroscopy Facility (ETSF), Unidad de Materiales Centro Mixto CSIC-UPV/EHU, Universidad del Pais Vasco, Avenida de Tolosa 72, E-20018 Donostia, Spain*

[4]*Institut für Festkörperphysik, TU Dresden, Mommsenstrasse 13, D-01069 Dresden, Germany*

[5]*Helmholtz-Zentrum Berlin, Albert-Einstein-Strasse 15, 12489 Berlin, Germany*

(Received 9 February 2009; revised manuscript received 6 April 2009; published 8 May 2009)

We propose graphite intercalation compounds (GICs) as a material system with precisely the same electronic properties as doped few layer graphene. Despite the fact that GICs have been around for the last four decades, this fact has gone unnoticed so far. Especially, we focus on the electronic energy bands of KC_8 which correspond to a doped graphene monolayer. We provide extensive theoretical and experimental evidence for this claim employing a combined angle-resolved photoemission and theory approach using tight-binding, standard density-functional theory and including electron-electron correlation on a *GW* level. We observe a strong momentum-dependent kink in the quasiparticle dispersion at 166 meV highlighting electron-phonon coupling to an in-plane transversal optical phonon. These results are key for understanding both the unique electronic properties of doped graphene layers and superconductivity in KC_8.

DOI: 10.1103/PhysRevB.79.205106 PACS number(s): 71.10.−w

I. INTRODUCTION

Graphite intercalation compounds (GICs) have been at the focus of intense research in the last four decades because they have a wide range of tunable electronic properties.[1] Especially, for stage I GICs, superconductivity was observed with transition temperatures T_C ranging from below 1 K for alkali-metal intercalation [e.g., 0.55 K for KC_8 (Ref. 2)] up to 11.5 K for CaC_6.[3] Interestingly, GICs also provide valuable insight into the electronic properties of doped few layer graphene (FLG). For example, a stage II(III) GIC has an electronic band structure most similar to a doped bilayer (trilayer) graphene.[4–6] In stage I alkali GICs, the graphene layers have *AA* stacking and only one π conduction (valence) band and can thus be considered as a doped graphene layer sandwiched in between two positively charged plates. Thus, the low-energy band structure of both stage I GICs and graphene are described by a 2×2 tight-binding (TB) Hamiltonian,[7,8] resulting in a linear π band dispersion close to the crossing point of the valence and conduction bands. The electronic band structure of GICs was also calculated by density-functional theory in the local-density approximation (LDA).[9] Experimentally, angle-resolved photoemission (ARPES) studies of GICs have been reported.[10,11]

Electron doping of GICs and FLG is carried out by intercalation of alkali or alkaline-earth metals and hole doping is done via intercalation of chlorides or fluorides such as $FeCl_3$ or AsF_5. Intercalation leads to a shift of the Fermi level (E_F) and the appearance of staging for higher intercalant concentrations. With increasing doping levels, the number of carriers increases which in turn increases electron-phonon coupling (EPC). This leads to the well-known appearance of superconductivity in GICs as EPC is the superconducting pairing mechanism.[3,12,13] Despite four decades of research, the story of GICs is not closed yet and until now the details in the low-energy quasiparticle (QP) dispersion of GICs regarding the superconducting coupling mechanism are not identified. Furthermore, the issue of whether the charge transfer to graphite is complete[14–17] or partial[10,11,18,19] was never resolved. Clearly, the charge transfer is reflected in the electronic band structure and can thus be in principle determined by ARPES. The phonon modes that mediate the superconducting coupling can in principle also be identified by ARPES as a kink in the QP dispersion; the energy of the kink is equal to the phonon energy. The details of the EPC are the key for understanding not only superconductivity but a range of other phenomena such as the double-resonance Raman effect and the transport in the high-bias regime in FLG transistors.

In this paper, we investigate the details of EPC in fully doped graphene monolayers in KC_8 using a combined first-principles and ARPES approach. We first provide theoretical results that clearly demonstrate the validity of the claim that the electronic structures of doped graphene and KC_8 are equivalent. We then provide arguments for the nearly complete charge-transfer state in KC_8 by doing partial self-consistent *GW* calculations. For practical applications, a set of third nearest-neighbor (3NN) TB parameters fit to *GW* and to the density-functional theory (DFT) calculations of doped graphene and KC_8 is provided. This is very useful for calculations of many properties (from transport to optical devices) where a proper description of the electronic structure is fundamental. We also use this set of parameters for a detailed comparison of *ab initio* calculations and the ARPES data. In the experimental part of the paper, we measure the quasiparticle band structure of KC_8 in the vicinity of the Fermi level by ARPES. We observe one valence and one conduction π band which are crossing in one point. This is precisely the electronic structure of a doped monolayer graphene. At 166 meV binding energy, we observe a kink in the quasiparticle

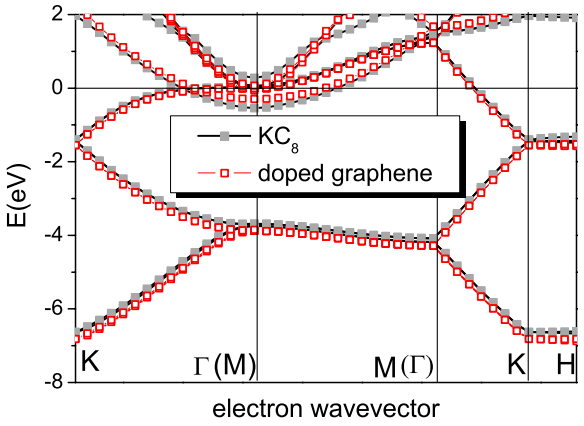

FIG. 1. (Color online) Calculated DFT band structure of KC_8 (gray lines) and electrostatic-doped graphene (red lines). The symmetry labels are for the Brillouin zones of KC_8 and doped graphene (in brackets). Note that in the doped graphene band-structure, the M point is folded into the Γ point of KC_8 (see also Ref. 19).

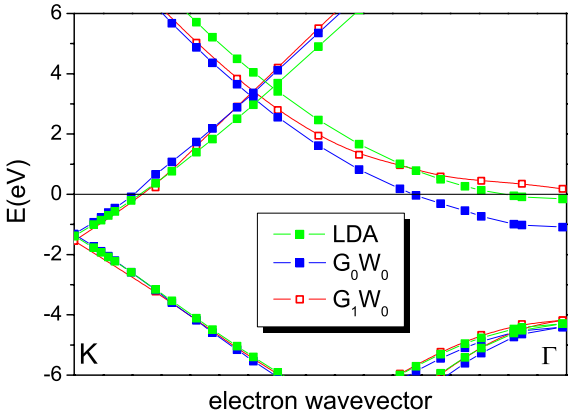

FIG. 2. (Color online) Band structure of the electrostatic doped graphene: LDA (green line), G_0W_0 (blue line), and G_1W_0 approximation (red line).

dispersion which is due to EPC. By a careful analysis of the observed kink, we unambiguously assign the kink in the ARPES spectra to EPC with an in-plane TO mode close to the K point. For a proper analysis of EPC, we use the 3NN TB description as the bare band dispersion. We also provide additional experimental data that supports the determination of the strength and anisotropy of λ, the EPC parameter.

II. *AB INITIO* CALCULATIONS OF ELECTROSTATICALLY DOPED GRAPHENE VERSUS KC_8

Here we show that the electronic dispersion close to the K point and the correlation effects in KC_8 can quantitatively be described by electrostatically doped graphene. Only minor differences related to the intercalation states are present close to E_F at the Γ point. The calculations of the electronic dispersion of graphene in a slab geometry ($d=20$ a.u.) are performed on two levels. First, we calculate the Kohn-Sham band structure within the LDA to DFT.[20] Wave functions are expanded in plane waves with an energy cutoff at 25 Ha. Core electrons are accounted for by Trouiller-Martins pseudopotentials. In the second step, we use the GW approximation[21–23] to calculate the self-energy corrections to the LDA dispersion.[24] For the calculation of the dielectric function $\epsilon(\omega,q)$, we use a Monkhorst-Pack k grid sampling $36\times36\times1$ points and bands up to 70 eV (namely, 50 bands) of the first Brillouin zone (BZ). In a further step, we performed GW calculations including partial self-consistency in G. Note that this is a conserving approximation whereas the single shot G_0W_0 is not. Calculations were performed using the code YAMBO.[24] More details for the first-principles calculations are given elsewhere.[25]

In Fig. 1, the band structure of KC_8 calculated within DFT is compared to the band structure of the electrostatic-doped graphene with the same atomic structure as KC_8. The comparison reveals that the band structure remains completely unchanged in the region close to the Dirac point. Differences are visible only close to the Fermi energy in the slope of the π^* bands that makes the size of the Fermi-energy surface larger in KC_8 and at Γ point where a deeper band coming from K is present in the case KC_8. Furthermore, in agreement with the experimental results discussed later, the dispersion along k_z (the KH line) is completely flat for the π bands. The absence of a k_z dispersion can be understood in terms of an increase in c, the interlayer spacing due to potassium intercalation. For graphite, $c=3.35$ Å but KC_8 has $c=5.30$ Å. The increase in c clearly reduces the wave-function overlap of atoms which are in adjacent graphene layers thereby lowering the out-of-plane bandwidth. Indeed, for graphite, a k_z dispersion is predicted theoretically and could be measured by ARPES.[26] However, in the case of KC_8, the wave-function overlap is too small to produce a finite k_z dispersion. This theoretical result is in agreement with the ARPES experiments as will be shown later.

Subsequently, in order to include correlation effects on the band structure, we performed a GW calculation (using the LDA wave functions as a starting point[26,27]) of the QP dispersions of doped graphene and the KC_8 structure (the same conclusions discussed above hold at this level of approximation). The LDA calculation predicts an incomplete charge transfer from potassium ions to graphene (in agreement with previous calculations; see, for example, Ref. 9 and references therein). However, the measured ARPES spectra taken around Γ point do not have any measurable intensity as shown in Ref. 28. Thus, from an experimental point of view, we would expect that all charge donated from the K ions goes into the π^* bands at K point. In order to clarify this discrepancy between the ARPES experiment and *ab initio* calculations, we investigated the impact of correlation effects at the GW approximation on the band structure at Γ. In particular, we studied the effect of partial self consistency in GW_0, without updating the wave functions, as the standard one-shot G_0W_0 does not give a full charge transfer. The rationale behind is that GW_0 in contrast to G_0W_0 is a conserving approximation[29] that is mandatory when addressing the physics close to E_F. Without losing of generality, we performed the GW approximation on electrostatically doped graphene. The result is shown in Fig. 2. It can be seen that the first iteration in G brings the band at Γ up to E_F leaving

TABLE I. Parameters of the 3NN tight binding fits to ARPES experiment, LDA, and GW calculations. γ_0^1, γ_0^2, and γ_0^3 are the in-plane hopping parameters for first to 3NN. The parameters s_0^1, s_0^2, and s_0^3 are the overlap integrals. The on-site energy is given by E_0. See, e.g., Ref. 4 (Fig. 1) for an illustration of the unit cell. These parameters were used to calculate the TB band structures from Figs. 3 and 4.

	Par.						
Method	γ_0^1	γ_0^2	γ_0^3	s_0^1	s_0^2	s_0^3	E_0
LDA KC_8	−3.253	−0.203	−0.558	0.108	0.032	0.077	1.880
GW KC_8	−3.218	−0.257	−0.562	0.252	0.0793	0.110	1.834
LDA graphene	−3.261	−0.219	−0.529	0.079	0.0381	0.055	1.885
GW graphene	−3.304	−0.219	−0.471	0.092	0.029	0.049	1.863

the band structure close to K unaltered; a subsequent interaction in G did not result in any further changes in the band structure. This indicates that electron-electron interaction dictates the nearly full charge transfer. The agreement between calculated QP band structure and experiments is very good once G_1W_0 is performed, while with a single-shot G_0W_0 the QP results for KC_8 and electrostatically doped graphene disagree with the experiments due to the presence of the K 4*s* bands at the Γ point. However, this band moves up and eventually crosses E_F once self-consistency in G is performed. This indicates an initial overestimation of exchange correlation effects in the extended homogeneously distributed intercalated K band (as it is originally occupied in the starting LDA band structure). Therefore, in agreement with our ARPES experiments we found evidence for an almost complete charge transfer (also found in Ref. 30).

III. TIGHT-BINDING DESCRIPTION OF DOPED GRAPHENE LAYERS IN KC_8

Since both the LDA and *GW* calculations are computationally expensive and for most relevant applications (transport, optical absorption, etc.) many k points of the band structure are needed, we performed a TB fit of the *ab initio* data that can be used in a wide range of situations (including having reliable bare-band dispersion for the self-energy analysis of the EPC, as will be discussed later). The 3NN-TB model was employed to fit the experimental and calculated data. It has already been shown in our previous works for both pristine and doped graphene layers that the 3NN interactions are crucial for describing the electronic energy-band structure.[4,31] We stress here that the first nearest-neighbor TB model (as it was previously used in the literature) is not sufficient to describe the electron energy dispersions of KC_8, especially the trigonal warping effect cannot be well reproduced. The details of the 3NN TB model are given in Ref. 4. In short, we have three in-plane hopping matrix elements γ_0^1, γ_0^2, and γ_0^3 and corresponding overlap matrix elements s_0^1, s_0^2, and s_0^3. The on-site matrix elements are denoted by E_0. We have performed fits of the 3NN TB parameters to all four *ab initio* calculations (LDA and *GW* of KC_8 and doped graphene). The parameters that reproduce the *ab initio* calculations are reported in Table I. When comparing the parameters to our previous fit to pristine graphene layers,[4] some modifications of the hopping parameters highlight that the doping not only shifts the Dirac point to the π^* band but also changes the band structure. In particular, the higher electron density increases screening and, thus, the Fermi velocity becomes smaller which is reflected in a decrease (increase) in the absolute value of $\gamma_0^1(\gamma_0^3)$ (note that $3\gamma_0^1-\gamma_0^3$ is proportional to the Fermi velocity[32,33]).

The *ab initio* calculated points and the fits that reproduce this approach are shown in Fig. 3. It can be seen clearly that the *GW* calculation of doped graphene has the steepest bands (smallest Fermi surface) and the LDA calculation of KC_8 has the flattest bands (or the largest Fermi surface). The trigonal warping effect is largest for the LDA calculations of KC_8, whereas it is smallest for the *GW* calculation of doped graphene. This is because the partial hybridization of carbon and potassium states increases the difference between the velocity along the *KM* and *K*Γ directions. It is interesting to compare the *GW* calculations of doped graphene to the case of undoped graphene sheets, for which the Fermi level is shifted rigidly by 1.35 eV. This emphasizes small differences in the shape of the electronic bands at E_F between undoped and doped graphenes. Due to the fact that in doped graphene the particle-hole symmetry is not valid anymore, the renormalization of the band velocity is different for conduction and valence bands at the *GW* level. This puts in evidence the limitations of the simple electrostatically doped model of shifting E_F rigidly to mimic the doping level once we go away from the neutrality Dirac point of graphene. These deviations are related to the increase in the trigonal warping effect with doping introduced by electron correlations.

The comparison between the Dirac cones is shown in Fig. 4 and the increase in the trigonal warping effect of the conduction band at E_F can be clearly seen. This is of importance for gated graphene devices in a field-effect transistor geometry since the stronger trigonal warping effect would enhance the curvature of the bands in *KM* direction. As this deviation is stronger close to E_F, it does not affect our conclusions concerning the Dirac point of graphene. The band-dispersion close to the Dirac point is very much the same for doped and undoped graphenes.

IV. EXPERIMENTAL

Experiments were done at BESSY II using the UE112-PGM2 beamline and a Scienta RS 4000 analyzer yielding a

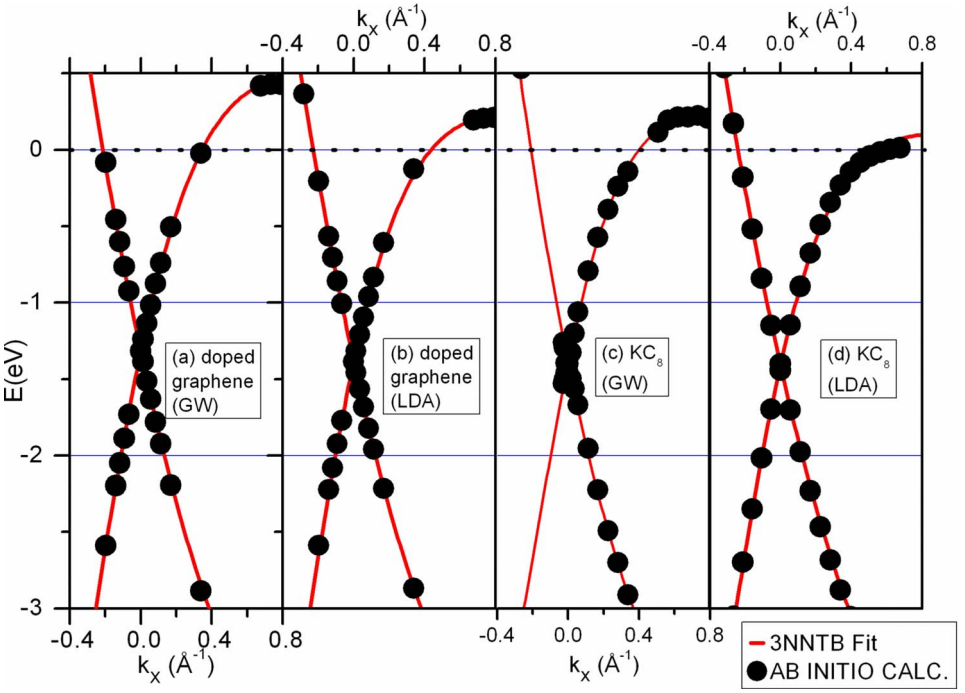

FIG. 3. (Color online) Fits of the *ab initio* results (black points) by 3NN tight-binding calculations (red lines). See Table I for the TB parameters used here.

total-energy resolution of 15 meV and a momentum resolution better than 0.01 $Å^{-1}$. All photoemission spectra were taken at a photon energy of 48 eV. Natural graphite single-crystal samples (~1 cm in diameter) were mounted on a three-axis manipulator and cleaved *in situ*. Intercalation was performed using commercial SAES getter sources dosing potassium at 6.3 A for several minutes. Subsequent steps of evaporation with the graphite sample at room temperature were followed by equilibration for 30 min at 50 °C. The distance from the getter source was 7 cm and the total dosing time was 50 min. In order to check the doping level, we measured ARPES after each intercalation step. The proof that we reached stage I was given by the appearance of only one π valence band [instead of 2(3) valence bands for stages II(III)]. In addition, stage I compounds are identified by their characteristic golden color and a 2×2 in-plane reconstruction as observed by the low-energy electron diffraction. Additional evaporation of potassium did not further increase the doping level. After full intercalation, KC_8 was immediately cooled down by liquid He to ~25 K and measured.

In Fig. 5(a), the ARPES intensity for a cut through the *K* point is shown along with the TB fits to the experiments (Refs. 28) and TB-*GW* calculations for doped graphene as discussed earlier (using the parameters in Table I). It is evident that the TB-*GW* calculation fits well the maxima of the experimental ARPES intensity. Therefore, we will use this TB calculation as the bare electronic energy-band structure for analyzing the EPC as will be discussed later. The momentum distribution curves (MDCs) for the same cut are shown in Fig. 5(b) along with the Lorentzian fits of the maxima of the spectral function. It can be seen that the spectral function is approximated well by Lorentzians both above and below the kink energy. From the positions and widths of the Lorentzians, the spectral function can be extracted which

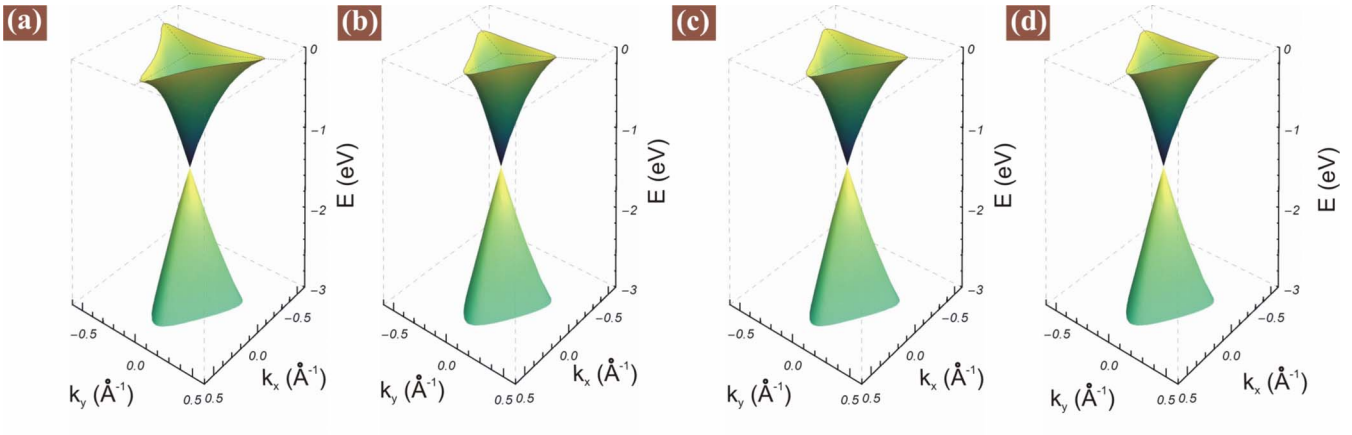

FIG. 4. (Color online) Dirac cone for KC_8 calculated by (a) TB-LDA and (b) TB-*GW* and the Dirac cone of doped graphene by (c) TB-LDA and (d) TB-*GW*. Parameters are given in Table I.

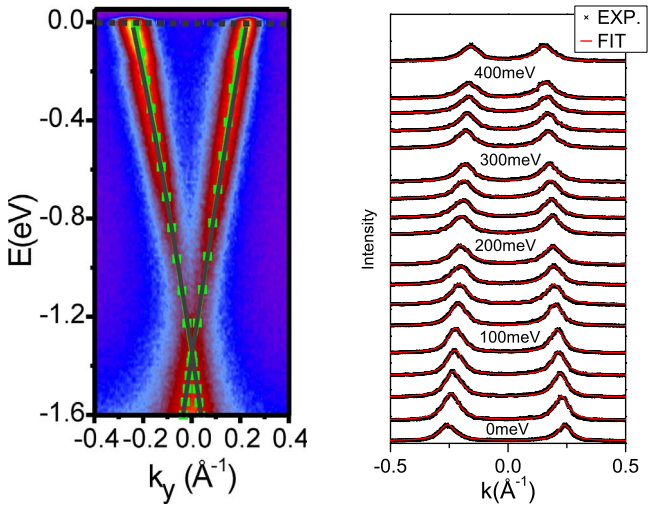

FIG. 5. (Color online) (Left panel) ARPES intensity of KC_8 of the scan through the K point. The full line and boxes denote TB fits to experiment and the TB-GW calculation of doped graphene, respectively. (Right panel) MDC scans at different binding energies and the Lorentzian fits.

is directly related to coupling of electrons to phonons, plasmons, etc. In Sec. V, we will make use of both the positions and widths of the Lorentzians in order to evaluate the EPC.

It is evident that we have only one π valence and one π conduction band and that they meet in one point, i.e., the Dirac point. Note that this situation is completely different to the case of pristine graphite, where two π valence and conduction bands are observed.[26] Thus, the electronic band structure of a doped graphene monolayer and KC_8 is identical and one can measure KC_8 in order to study graphene without the complications introduced by the substrate interaction.

V. ANALYSIS OF ELECTRON-PHONON COUPLING

We perform an analysis of the EPC parameter, λ from the Lorentzian MDCs shown in Fig. 5(b). We obtain λ in a self-consistent manner from both the width (related to the imaginary part of the self energy, $\mathrm{Im}\,\Sigma$) and the position of the Lorentzians (related to the real part of the self energy, $\mathrm{Re}\,\Sigma$).[34,35] The evaluation of λ from $\mathrm{Im}\,\Sigma$ does not depend on the details of the dispersion of the bare QP bands. In order to get λ from $\mathrm{Re}\,\Sigma$, one needs a bare energy-band dispersion which does not contain electron-phonon interactions. For this purpose, we employed the TB-GW description as laid out earlier. The EPC is related to $\mathrm{Im}\,\Sigma$ by

$$\lambda = \frac{2\,\mathrm{Im}\,\Sigma}{\hbar\omega_{ph}\pi}. \tag{1}$$

Here, $\hbar\omega_{ph}$ denotes the phonon energy and $\mathrm{Im}\,\Sigma$ denotes the step height of the imaginary part of the self-energy at a binding energy of $\hbar\omega_{ph}$. The size of the λ is also directly proportional to the slope of $\mathrm{Re}\,\Sigma$ at E_F, i.e.,

$$\lambda = -\left.\frac{\partial\,\mathrm{Re}\,\Sigma(E)}{\partial E}\right|_{E=E_F}. \tag{2}$$

Our doping-dependent experiments reveal that the energy of the kink is independent of the doping level and thus it cannot be explained by electron-plasmon coupling. This is a strong hint for that the observed kink is indeed coming from photohole relaxation by phonon emission, i.e., EPC. It is clear that a photohole can relax to a lower binding-energy state by EPC in two ways by intravalley and intervalley scatterings. The intravalley (purple) and intervalley (blue) decay processes are shown schematically in Fig. 6(a), respectively. From momentum considerations, it is clear that intravalley (intervalley) scattering would couple with the Γ point (K point) phonons, which clearly have a different energy. In contrast to previous works, which rely on the intravalley scattering process around K or K' points and the emission of phonons close to the Γ point,[36] our data unambiguously identify the mechanism of photohole decay as intervalley scattering between K and K' points with the emission of a phonon close to the K point. In Fig. 6(b), we schematically illustrate this mechanism in the two-dimensional (2D) BZ of graphene with the exchange of a phonon with wave vector $q(K)$. In Fig. 6(c), we show the region of the π band close to the Fermi level enlarged. On top of the ARPES data, we show the maxima of the MDCs and the bare energy-band structure (from the TB fits). Clearly the band has a strong kink below the Fermi energy at a value that is equal to the K point phonon energy in graphite. For precise determination of the kink energy, we extracted $\mathrm{Im}\,\Sigma$ and $\mathrm{Re}\,\Sigma$ from the MDCs as described above in Eqs. (1) and (2). If we were only dealing with coupling to a single Einstein phonon then $\mathrm{Re}\,\Sigma$ should have a peak and $\mathrm{Im}\,\Sigma$ a jump at the energy of the coupling phonon mode.[34] Indeed, this is what we observed as shown in Fig. 6(d), indicating that the physical process behind the kink is dictated by the strong EPC. The exact energy of the kink is analyzed from the peak of $\mathrm{Re}\,\Sigma$ and the step energy of $\mathrm{Im}\,\Sigma$. We find self-consistently that $\mathrm{Re}\,\Sigma$ has a peak at 166 meV and $\mathrm{Im}\,\Sigma$ has a step at 166 meV. Looking at the phonon-dispersion relation, we can identify the coupling phonons clearly as K-point phonons as the energy of Γ point phonons is too large (196 meV) to explain the observed kink. In the Appendix, we provide further information on the calculation of the phonon energies.

From $\mathrm{Im}\,\Sigma$ we can furthermore extract β, the electron-electron coupling which is the coefficient of the quadratic Fermi-liquid energy dependence of $\mathrm{Im}\,\Sigma$. In the following, we perform an analysis of the directional-dependent coefficients λ and β as a function of the angle ϕ between the KM to the $K\Gamma$ directions. As can be seen in Fig. 6(e), the λ extracted from $\mathrm{Re}\,\Sigma$ and $\mathrm{Im}\,\Sigma$ is in good agreement concerning the anisotropy of the coupling, although the actual size of the coupling differs by about 20%. The resulting EPC is maximum close to the KM direction and minimum in the $K\Gamma$ direction. Interestingly, regarding the Fermi liquidlike electron-electron coupling β, which is also depicted in Fig. 6(e), we observe the same anisotropy in β as for λ. This direction dependence of β reflects the anisotropy of the QP-band structure close to E_F and highlights that there is an

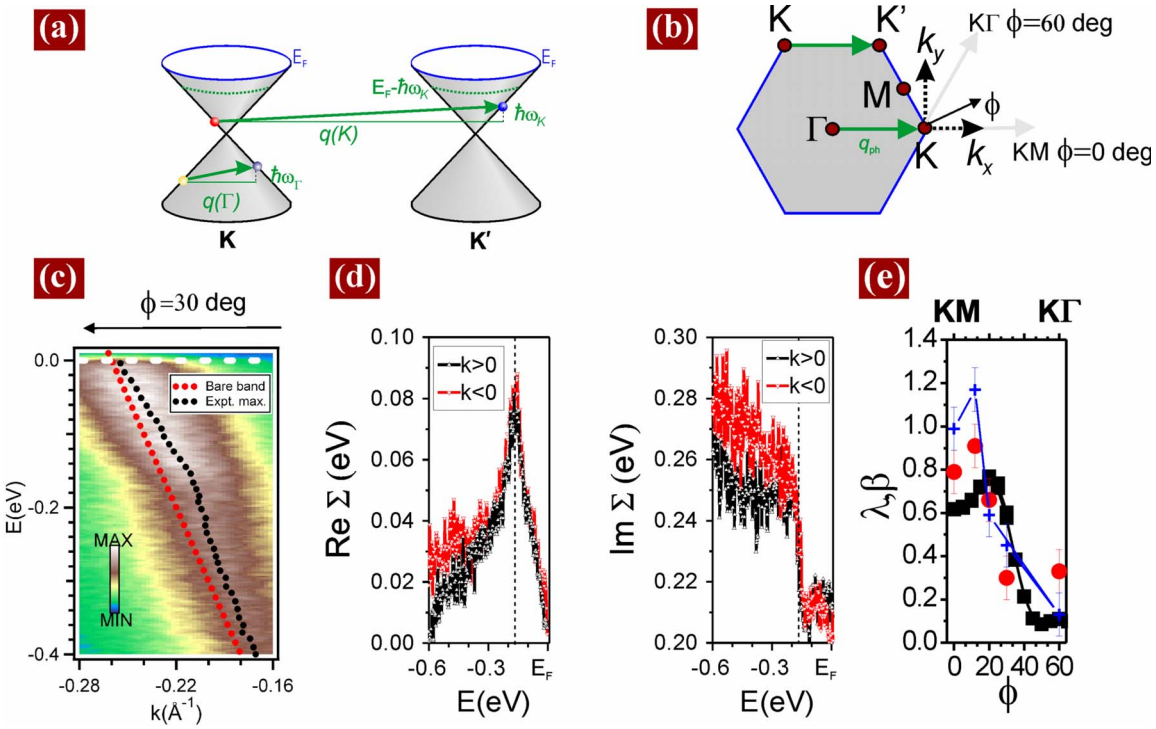

FIG. 6. (Color online) (a) Schematics of the photohole scattering process from K to K' by EPC to a K-point phonon with energy $\hbar\omega_K$. The initial and final photohole states around K and K' are denoted by circles. The arrow denotes the exchanged phonon with wave vector $q(K)$ and energy $\hbar\omega_K$ which is emitted by photohole relaxation. Additionally, we show photohole relaxation by emission of Γ point phonons. In this case, the initial and final photohole state are around the same K point. (b) 2D-BZ indicating the phonon wave vector $q(K)$. (c) Measured ARPES intensity in the region of the kink. A straight dashed line denotes the bare band dispersion and a kinked dotted line is the experimental MDC maxima. (d) Real and imaginary part of the self-energy. (e) The angular dependence of the EPC constant λ and the electron-electron correlation constant β; black squares (red circles) denote λ extracted from the measured real (imaginary) part of the self-energy. β is denoted by blue crosses.

intrinsic electronic origin of the anisotropy. Therefore, the minor anisotropy of λ as obtained in our calculation and in previous DFT calculations[37,38] as compared to the one extracted here from ARPES clearly indicates a need of going beyond LDA to describe exchange and correlation effects in the QP energies and wave functions.[39,40] This argument is supported by our finding that self-energy corrections at the *GW* level are needed to describe the observed absence of ARPES intensity at Γ, in contrast to what is predicted by LDA. Finally, in Fig. 7 we show the experimentally observed Lorentzian widths for different angles ϕ from which we extract Im Σ and thus λ and β. The data are collected at the high-symmetry directions along $K\Gamma$ and KM and in between. The binding energy-dependence Im Σ is fit by a steplike function plus a quadratic binding-energy dependence (const $+\beta E^2$) in order to obtain λ and β. It can be seen that both λ and β increase significantly toward the KM direction.

VI. DISCUSSION AND CONCLUSIONS

In summary, we have shown by a comprehensive comparison of the electron energy-band dispersions that KC_8 is indeed equivalent to a doped graphene monolayer. This finding provides an elegant solution to the substrate interaction which is known to open up a gap at K point. The magnitude of the gap depends crucially on the substrate; for graphene

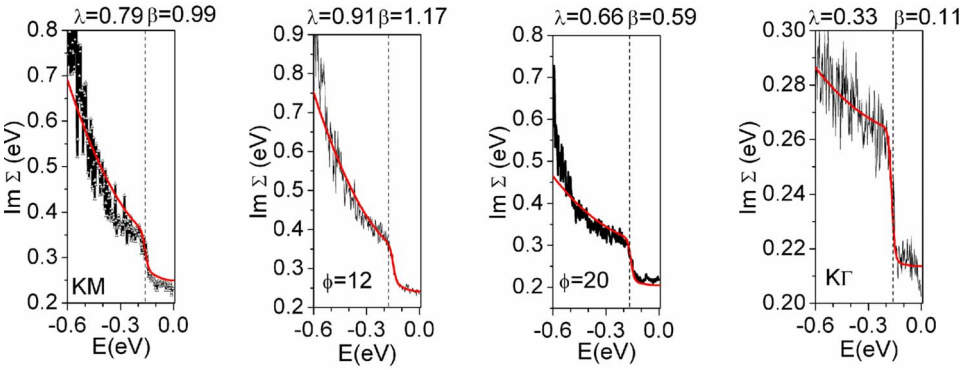

FIG. 7. (Color online) Im Σ as a function of binding energy for different angles around the K point. The red line denotes Im Σ as calculated from the fit of λ and β. Note the different energy scales for Im Σ.

on Ni(111) it is ~1 eV (Ref. 41) but for graphene on SiC (silicon phase) the gap is ~0.26 eV.[42] Notably for graphene on the carbon phase of SiC, the gap might even be in the meV range. Also, in the case of bulk graphite with *AB* stacking, experiments that probe the gap at the *H* point yield a value in the order of a few meV.[4,26] Nevertheless in all cases, the electrons acquire a finite rest mass and the concept of Dirac Fermions breaks down. However, in the case of KC_8, the stacking sequence is changed to *AA* stacking and the arrangement of K atoms is such that it does not induce a gap.

Furthermore, the QP-band structure was discussed theoretically in detail in connection with the charge-transfer problem (complete versus incomplete), and it showed the importance to go beyond the G_0W_0 approximation. The charge-transfer problem (complete versus incomplete) illustrates the need to go beyond G_0W_0-type calculations.

Most importantly, we have observed a kink feature in the quasiparticle dispersion which is in agreement to previous results on doped graphene.[43] Our analysis of the kink does not suffer from an overestimation of λ in *KM* direction.[43,44] The kink feature was assigned to EPC to a *K*-point phonon of the transverse optical (TO) branch. Since EPC is the driving mechanism for a superconductivity, we can discuss the possible implications for the superconducting pairing mechanism in GICs. By an accurate comparison to the graphite phonon-dispersion relation,[45–47] we can unambiguously assign the kink to a coupling to the in-plane transverse optical (iTO) phonon branch near the *K* point. This argument is supported by the fact that the electron-phonon coupling matrix element with the iTO phonons is much stronger than with other branches[37,39,48] and that the phonon density of states (DOS) is strongly peaked due to the flat dispersion of the iTO branch around *K*.

Interestingly, a very similar process for scattering of photoexcited electrons is the origin for the very intense *G'* band in the double resonance Raman process in sp^2 hybridized carbon materials. The difference between the photohole scattering (ARPES) and photoexcited electron scattering (resonance Raman) is that the photohole is created below the Fermi level and the photoexcited electron is generated above the Fermi level by a dipole transition from the valence band. The strong EPC also limits the maximum bias current through graphene-based nanoelectronic devices and provides an upper bound for the phonon-mediated BCS superconductivity of KC_8. In classical BCS theory, the transition temperature T_c is evaluated using the McMillan formula[49]

$$T_C = 0.69\Theta \exp\left(-\frac{1.04(\lambda+1)}{\lambda-(0.62\lambda+1)\mu^*}\right). \quad (3)$$

Here, we use the measured energy of the kink $\hbar\omega = 166$ meV which is converted to a phonon temperature $\Theta = 1926$ K and our measured average EPC constant of $\lambda = 0.45$ and a screened pseudopotential $\mu^\star \sim 0.14$.[13] These values would allow a $T_c \sim 5$ K. Such a tendency of the McMillan formula to give an upper limit for T_c is well known and a result of the following facts: we use an Einstein phonon and not the Eliashberg formula which includes the full phonon-dispersion relation; we use an averaged electron-phonon coupling constant and the value of the screened pseudopotential μ^* is generally not well known and this is also the case for KC_8. In addition, there are Cooper pair breaking effects. These remaining differences to the experimental T_c can be explained by either uncertainties in $\mu^\star$ by additional not yet known pair breaking effects and/or by additional coupling to other electron and phonon branches.[3,13] This highlights that in agreement with previous theoretical studies,[3,13] the superconductivity in GIC very sensitively depends on details of the band structure at low-energy scale and the presence or absence of intercalated-derived partially-filled bands. The question why different alkali GICs have different values of T_c arises. There are several parameters, which are intercalant specific and crucially affect T_c. First, different alkali (or alkaline) earth metals have different amounts of charge transfer per intercalant atom. This in turn affects the DOS at the Fermi level and hence EPC which enters into the McMillan formula for T_c. Second, the differences in the values of T_c for different alkali metal-doped GICs can also arise from slightly different values of μ^*, a different phonon-dispersion relation, and also Cooper pair breaking effects.

ACKNOWLEDGMENTS

A.G. acknowledges an APART Fellowship from the Austrian Academy of Sciences and a Marie Curie Individual Fellowship (COMTRANS) from the European Union. T.P. acknowledges DFG under Project No. PI 440/3/4/5. C.A. and A.R. acknowledge funding by the Spanish MEC (Grant No. FIS2007-65702-C02-01), "Grupos Consolidados UPV/EHU del Gobierno Vasco" (Grant No. IT-319-07), and the European Community through NoE Nanoquanta (Grant No. NMP4-CT-2004-500198), e-I3 ETSF Project (INFRA-2007-1.2.2: Grant No. 211956), and SANES (Grant No. NMP4-CT-2006-017310). The computer resources were provided by the Barcelona Supercomputing Center and the Basque Country University UPV/EHU (SGIker Arina) and ETSF. D.V. acknowledges DFG under Project No. VY64/1-1. J.F. acknowledges and appreciates financial support by the DFG (Forschergruppe No. FOR 538).

APPENDIX

In the remaining paragraph, we provide further theoretical evidence for the phonon mode assignment. In order to understand which phonon is responsible of the kink in the quasiparticle band structure of the KC_8, we studied the two pos-

TABLE II. Calculated optical phonon energies for the in-plane TO phonon branch at Γ and *K* points for pristine and doped graphene with and without nonadiabatic (NA) effects.

	Energy meV (cm^{-1})	
System	Γ	K
Pristine graphene	194.5(1569)	164.4(1326)
Doped graphene	154.7(1248)	169.8(1370)
Doped graphene +NA effects	195.8(1579)	170.2(1373)

sible phonons from Γ and *K* points. Three main effects are considered that affect the bare phonon frequencies in order to discern which phonon is responsible for the measured kink at 166 meV. These three effects are (1) doping dependence, (2) EPC, and (3) nonadiabatic effects. We analyzed the phonons of a doped graphene sheet with the lattice constants from KC_8 (Ref. 50) and showed the calculated results in the Table II. The first effect on the phonon frequencies is due to the doping that reduces the phonon frequencies at Γ and increases the ones at *K* point. The second effect is due to correlation, namely, the fact that LDA fails to reproduce the correct EPC. We studied correlation effects on the electron-phonon matrix elements, at the *GW* level as described in Ref. 40 and we found that in the case of doped graphene these cause an increase of about 10% of the phonon frequencies, in contrast to the undoped case where the increase was up to 60% for the *K* phonon. As a third effect, we considered nonadiabatic effects on the phonon as described in Ref. 51, and in agreement with Ref. 52). The inclusion of nonadiabatic effects in the phonon calculation is particularly relevant for the Γ phonons, while for the *K*-point phonons the effect of correlation is smaller and less doping dependent. As one can see in Table II the shift due to the doping and the nonadiabatic effects mainly cancel each other for the Γ-point phonons. Our results clearly show that the only possible phonon for the kink in the KC_8 QP dispersion is the in-plane TO phonon from the *K* point. Experimentally, the Γ-point phonons of KC_8 have been measured by Raman[53,54] yielding a phonon frequency of 192 meV (1547 cm^{-1}). This is another experimental proof that the coupling phonon does not come from Γ point and hence must come from the *K* point.

[1] M. S. Dresselhaus and G. Dresselhaus, Adv. Phys. **30**, 139 (1981).
[2] N. B. Hannay, T. H. Geballe, B. T. Matthias, K. Andres, P. Schmidt, and D. MacNair, Phys. Rev. Lett. **14**, 225 (1965).
[3] G. Csanyi, P. B. Littlewood, Andriy H. Nevidomskyy, C. J. Pickard, and B. D. Simons, Nat. Phys. **1**, 42 (2005).
[4] A. Grüneis, C. Attaccalite, L. Wirtz, H. Shiozawa, R. Saito, T. Pichler, and A. Rubio, Phys. Rev. B **78**, 205425 (2008).
[5] Sylvain Latil and Luc Henrard, Phys. Rev. Lett. **97**, 036803 (2006).
[6] B. Partoens and F. M. Peeters, Phys. Rev. B **74**, 075404 (2006).
[7] J. Blinkowski, N. H. Hau, C. Rigaux, J. P. Vieren, R. L. Toullec, G. Furdin, A. Herold, and J. Melin, J. Phys. (France) Lett. **41**, 47 (1980).
[8] R. Saito and H. Kamimura, Phys. Rev. B **33**, 7218 (1986).
[9] K. Rytkönen, J. Akola, and M. Manninen, Phys. Rev. B **75**, 075401 (2007).
[10] W. Eberhardt, I. T. McGovern, E. W. Plummer, and J. E. Fischer, Phys. Rev. Lett. **44**, 200 (1980).
[11] N. Gunasekara and T. Takahashi, Z. Phys. B: Condens. Matter **70**, 349 (1988).
[12] K. Sasaki, J. Jiang, R. Saito, S. Onari, and Y. Tanaka, J. Phys. Soc. Jpn. **76**, 033702 (2007).
[13] M. Calandra and F. Mauri, Phys. Rev. Lett. **95**, 237002 (2005).
[14] G. Wang, W. R. Datars, and P. K. Ummat, Phys. Rev. B **44**, 10880 (1991).
[15] M. T. Johnson, H. I. Starnberg, and H. P. Hughes, Solid State Commun. **57**, 545 (1986).
[16] J. Algdal, T. Balasubramamian, M. Breitholtz, T. Kihlgren, and L. Wallden, Surf. Sci. **601**, 1167 (2007).
[17] J. M. Zhang and P. C. Eklund, J. Mater. Res. **2**, 858 (1987).
[18] P. Oelhafen, P. Pfluger, E. Hauser, and H. J. Guntherodt, Phys. Rev. Lett. **44**, 197 (1980).
[19] T. Inoshita, K. Nakao, and H. Kamimura, J. Phys. Soc. Jpn. **43**, 1237 (1977).
[20] X. Gonze, J. M. Beuken, R. Caracas, F. Detraux, M. Fuchs, G. M. Rignanese, L. Sindic, M. Verstraete, G. Zerah, F. Jollet, M. Torrent, A. Roy, M. Mikami, Ph. Ghosez, J. Y. Raty, and D. C. Allan, Comput. Mater. Sci. **25**, 478 (2002).
[21] M. S. Hybertsen and S. G. Louie, Phys. Rev. B **34**, 5390 (1986).
[22] L. Hedin, Phys. Rev. **139**, A796 (1965).
[23] S. G. Louie, *Topics in Computational Materials Science*, edited by C. Y. Fong (World Scientific, Singapore, 1997), p. 96.
[24] A. Marini *et al.*, the YAMBO project, http://www.yambo-code.org/
[25] C. Attaccalite, A. Grüneis, T. Pichler, and A. Rubio, arXiv:0808.0786 (unpublished).
[26] A. Grüneis, C. Attaccalite, T. Pichler, V. Zabolotnyy, H. Shiozawa, S. L. Molodtsov, D. Inosov, A. Koitzsch, M. Knupfer, J. Schiessling, R. Follath, R. Weber, P. Rudolf, L. Wirtz, and A. Rubio, Phys. Rev. Lett. **100**, 037601 (2008).
[27] Calculation performed with YAMBO code, arXiv:0810.3118 (unpublished).
[28] A. Grüneis *et al.*, Phys. Rev. Lett. (to be published).
[29] A. Schindlmayr, Phys. Rev. B **56**, 3528 (1997).
[30] D. P. DiVincenzo and S. Rabii, Phys. Rev. B **25**, 4110 (1982).
[31] A. Grüneis, C. Attaccalite, A. Rubio, D. Vyalikh, S. L. Molodtsov, J. Fink, R. Follath, W. Eberhardt, B. Büchner, and T. Pichler, arXiv:0808.1613 (unpublished).
[32] C. T. White, J. W. Li, D. Gunlycke, and J. W. Mintmire, Nano Lett. **7**, 825 (2007).
[33] D. Gunlycke and C. T. White, Phys. Rev. B **77**, 115116 (2008).
[34] J. Fink, A. Koitzsch, J. Geck, V. Zabolotnyy, M. Knupfer, B. Buchner, A. Chubukov, and H. Berger, Phys. Rev. B **74**, 165102 (2006).
[35] D. V. Evtushinsky, A. A. Kordyuk, S. V. Borisenko, V. B. Zabolotnyy, M. Knupfer, J. Fink, B. Buchner, A. V. Pan, A. Erb, C. T. Lin, and H. Berger, Phys. Rev. B **74**, 172509 (2006).
[36] A. Bostwick, T. Ohta, T. Seyller, K. Horn, and E. Rotenberg, Nat. Phys. **3**, 36 (2007).
[37] Matteo Calandra and Francesco Mauri, Phys. Rev. B **76**, 205411 (2007).
[38] C. H. Park, F. Giustino, J. L. McChesney, A. Bostwick, T. Ohta, E. Rotenberg, M. L. Cohen, and S. G. Louie, Phys. Rev. B **77**, 113410 (2008).
[39] D. M. Basko and I. L. Aleiner, Phys. Rev. B **77**, 041409(R) (2008).
[40] M. Lazzeri, C. Attaccalite, L. Wirtz, and F. Mauri, Phys. Rev. B **78**, 081406(R) (2008).

[41] A. Grüneis and D. V. Vyalikh, Phys. Rev. B **77**, 193401 (2008); A. Grüneis *et al.*, arXiv:0904.3220 (unpublished).
[42] S. Y. Zhou, G. H. Gweon, A. V. Fedorov, P. N. First, W. A. de Heer, D. H. Lee, F. Guinea, A. H. Castro Neto, and A. Lanzara, Nature Mater. **6**, 916 (2007).
[43] J. L. McChesney, A Bostwick, T Ohta, K. V. Emtsev, T Seyller, K. Horn, and E Rotenberg, arXiv:0705.3264 (unpublished).
[44] T. Valla, J. Camacho, Z.-H. Pan, A. V. Fedorov, A. C. Walters, C. A. Howard, and M. Ellerby, Phys. Rev. Lett. **102**, 107007 (2009).
[45] A. Grüneis, R. Saito, T. Kimura, L. G. Cançado, M. A. Pimenta, A. Jorio, A. G. Souza Filho, G. Dresselhaus, and M. S. Dresselhaus, Phys. Rev. B **65**, 155405 (2002).
[46] L. Wirtz and A. Rubio, Solid State Commun. **131**, 141 (2004).
[47] J. Maultzsch, S. Reich, C. Thomsen, H. Requardt, and P. Ordejon, Phys. Rev. Lett. **92**, 075501 (2004); A. Grüneis *et al.*, arXiv:0904.3205 (unpublished).
[48] M. Calandra and F. Mauri, Phys. Rev. B **76**, 161406(R) (2007).
[49] W. L. McMillan, Phys. Rev. **167**, 331 (1968).
[50] D. E. Nixon and G. S. Parry, J. Phys. C **2**, 1732 (1969).
[51] K. Ishioka, M. Hase, M. Kitajima, L. Wirtz, A. Rubio, and H. Petek, Phys. Rev. B **77**, 121402(R) (2008).
[52] A. M. Saitta, M. Lazzeri, M. Calandra, and F. Mauri, Phys. Rev. Lett. **100**, 226401 (2008).
[53] P. C. Eklund, G. Dresselhaus, M. S. Dresselhaus, and J. E. Fischer, Phys. Rev. B **16**, 3330 (1977).
[54] A. M. Rao, P. C. Eklund, S. Bandow, A. Thess, and R. E. Smalley, Nature (London) **388**, 257 (1997).